SUPPORTING INFORMATION

Non-Covalent Peptide Stapling Using Alpha-Methyl-L-Phenylalanine for Alpha-Helical Peptidomimetics

Ross A. D. Bathgate[#,*,1-3], Praveen Praveen[#,1], Ashish Sethi[#,3-5], Werner I. Furuya[1], Rishi R. Dhingra[1,2], Martina Kocan[1], Qinghao Ou[1], Adam L. Valkovic[1], Isis Gil-Miravet[6], Mónica Navarro-Sánchez[6], Francisco E. Olucha-Bordonau[6], Andrew L. Gundlach[1,2,7], K. Johan Rosengren[8], Paul R. Gooley[3,4], Mathias Dutschmann[1,2], and Mohammed Akhter Hossain[*,1,2,9]

[1]The Florey, The University of Melbourne, Parkville, VIC 3052, Australia, [2]Florey Department of Neuroscience and Mental Health, The University of Melbourne, Parkville, VIC 3052, Australia, [3]Department of Biochemistry and Pharmacology, The University of Melbourne, Parkville, VIC 3052, Australia, [4]Bio21 Molecular Science and Biotechnology, The University of Melbourne, Parkville, VIC 3052, Australia, [5]Australian Nuclear Science Technology Organisation, The Australian Synchrotron, Clayton, VIC 3168, Australia; [6]Predepartmental Unit of Medicine, Faculty of Health Sciences, Universitat Jaume I, Av. de Vicent Sos Baynat, s/n , 12071, Castelló de La Plana, Spain; [7]Department of Anatomy and Physiology, The University of Melbourne, Parkville, VIC 3052, Australia, [8]School of Biomedical Sciences, The University of Queensland, St Lucia, QLD 4072, Australia, [9]School of Chemistry, The University of Melbourne, VIC, Australia Parkville, VIC 3058.

S1. INTERACTION BETWEEN H3 RELAXIN, H3B10-27(13/17αF) AND RXFP3

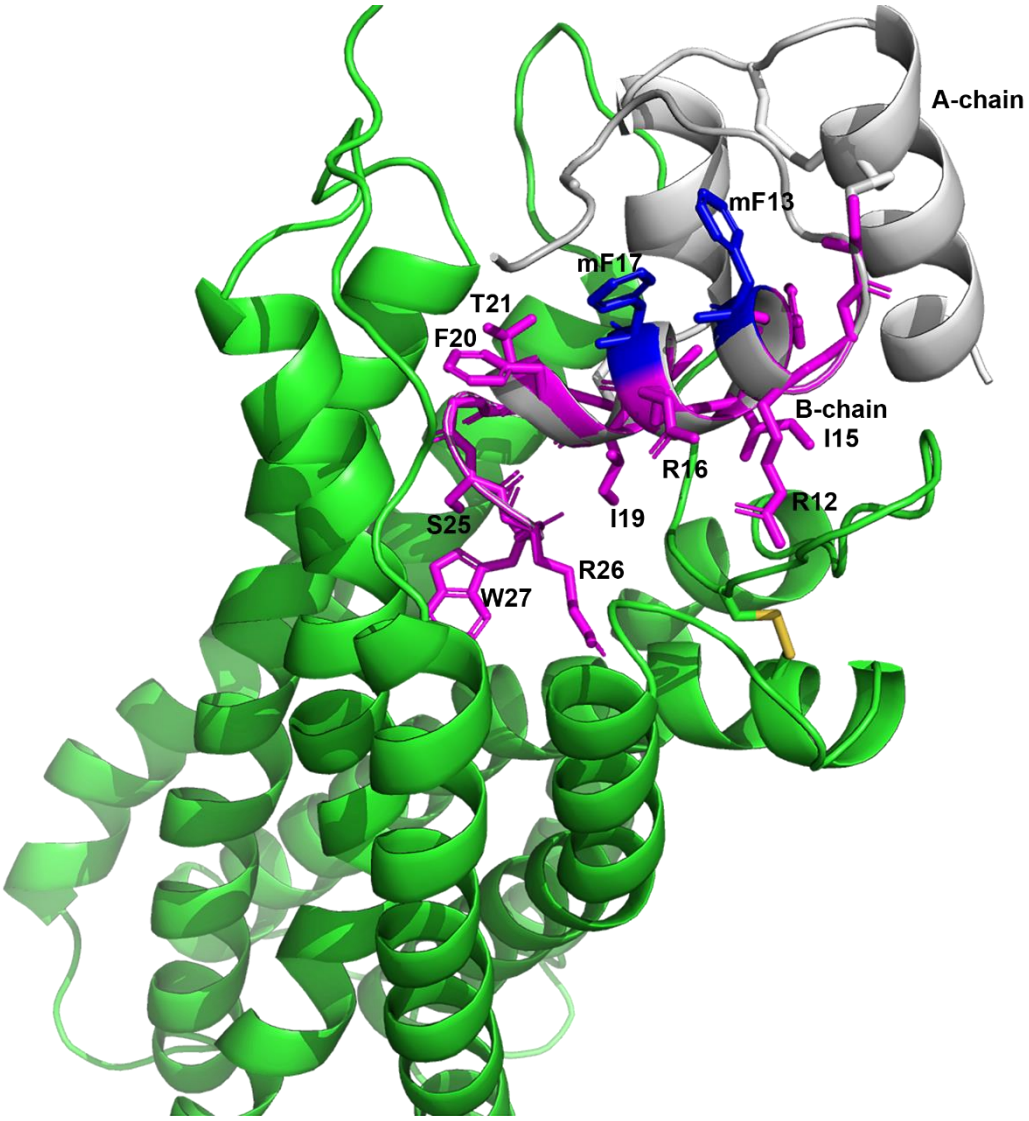

Figure S1. Model of H3 relaxin and its mimetic compound H3B10-27(13/17αF) bound to RXFP3. RXFP3 is shown in green and relaxin-3 in grey. This model is based on our previous extensive structure activity data on both relaxin-3 and RXFP3. Compound H3B10-27(13/17αF) is shown in magenta superimposed on the B-chain of relaxin-3. The key 'stapling residues' αF are shown in blue. Important sidechains involved in the RXFP3 interaction are labelled with residue numbers based on the relaxin-3 sequence.

S2. PEPTIDE SYNTHESIS AND CHARACTERIZATION

S2.1: Materials

Fluorenylmethoxycarbonyl (Fmoc) amino acids and O-(1H-6-chlorobenzotriazole-1-yl)-1,1,3,3-tetramethyluronium hexafluorophosphate (HCTU)/1-[Bis(dimethylamino)methylene]-1H-1,2,3-triazolo[4,5-b]pyridinium 3-oxide hexafluorophosphate (HATU) were purchased from GL Biochem (Shanghai, China). Fmoc-Trp (Boc) TentaGel S PHB resin (substitution 0.24 mmol/g), trifluoroacetic acid (TFA), and diisopropylethelene amine (DIEA) were purchased from Auspep (Melbourne, Australia). Acetonitrile, dichloromethane, piperidine (PPD), diethyl ether, N,N′-dimethylformamide (DMF) and methanol were purchased from Merck (Melbourne, Australia). Fmoc-α-methyl-L-phenylalanine was purchased from CHEM IMPEX INTERNATIONAL Inc (IL, 60191, United States). Triisopropylsilane (TIPS) anisole, sinapinic acid (3,5-dimethyl-4-hydroxycinnamic acid), DHB (2,5-dihydroxybenzoic acid) and human serum were purchased from Sigma-Aldrich (Sydney, Australia).

S2.2: Solid phase peptide synthesis

All single-chain peptides were synthesized using Fmoc solid phase synthesis on a microwave-assisted peptide synthesizer (CEM Liberty, Mathew, USA; Biotage (Sweden) Initiator+ Alstra microwave synthesizer) or manually using Fmoc protected L-α-amino acids. Peptide chains were assembled on preloaded resins. All side chain-protecting groups of amino acids were TFA-labile. The peptides were synthesized on either 0.1 or 0.2 mmol scale using instrument default protocols or manually with a 4-fold molar excess of Fmoc-protected amino acids activated by 4-fold excess of HCTU/HATU in the presence of excess (6-fold) DIEA. Nα-Fmoc protecting groups were removed by treating the resin-attached peptide with piperidine (20% v/v) in DMF. Using the microwave synthesizer, the coupling was conducted at 75°C using 25 W microwave power for 10 min for coupling and at room temperature for 5 min for deprotection. For manual synthesis, the coupling and deprotection were carried out for 60 min and 5 min three times, respectively. We have previously reported the synthetic methods for RXFP3 agonists, R3/I5[1], A2[2] and Peptide 5[3]. Specific details of the synthesis of the target peptide are elaborated in section S2.5 below.

S2.3: Peptide cleavage from the solid support

After completion of solid phase synthesis, peptides were cleaved using a cleavage cocktail of trifluoroacetic acid (TFA): TIPS: water: anisole (94: 1: 2: 3) for 2 h. Cleavage solution was filtered and evaporated under nitrogen. The cleaved peptide was precipitated in cold ether and centrifuged for 5 min; this step was repeated at least four times.

S2.4: Peptide purification and characterization by RP-HPLC and MALDI-TOF MS

RP-HPLC analysis and purification of the peptides were performed with Waters (Milford, MA 01757, United States) RP-HPLC systems or Shimadzu (Kyoto 604-8511, Japan) Nexera analytical RP-HPLC. Empower software for Waters was used for data collection, monitoring, and analysis.

Analysis: The analytical RP-HPLC profiles were acquired using a Phenomenex (Torrance, 411 Madrid Ave, United States) Gemini C18 analytical column (4.6 × 250 mm, pore size 110 Å, particle size 5 μm), at a constant flow rate of 1.5 mL/min, in a gradient mode with buffer A, 0.1% TFA in water, and buffer B, 0.1% TFA in acetonitrile, monitoring at a wavelength of 214 nm, which is characteristic for the amide bond.

Purification: All HPLC purifications were performed using a Phenomenex C18 preparative column (21.2 × 150 mm, pore size 110 Å, particle size 5 μm), at a constant flow rate of 10mL/min, in a gradient mode with eluent A, 0.1% TFA in water, and eluent B, 0.1% TFA in acetonitrile.

Peptide characterization was conducted on a Bruker Ultraflex II instrument (Bruker Daltonics, Bremen, Germany) MALDI-TOF MS (matrix-assisted laser desorption ionization time-of-flight mass spectrometry) and SHIMADZU MALDI-8020 (Kyoto 604-8511, Japan), Sinapinic acid and DHB in 0.1% TFA in ACN/water (7:3) was used as a matrix.

S2.5: Analytical RP-HPLC and MALDI-TOF-MS of purified peptides

S2.5.1: Analytical RP-HPLC and MALDI-TOF-MS of purified H3B10-27.

RP-HPLC was carried out as described above using the elution gradient: buffer B 25-55% for 30 min, t = 10.927 min.

MALDI-TOF-MS $[M+H]^+$ calculated 2026.264, observed 2029.436.

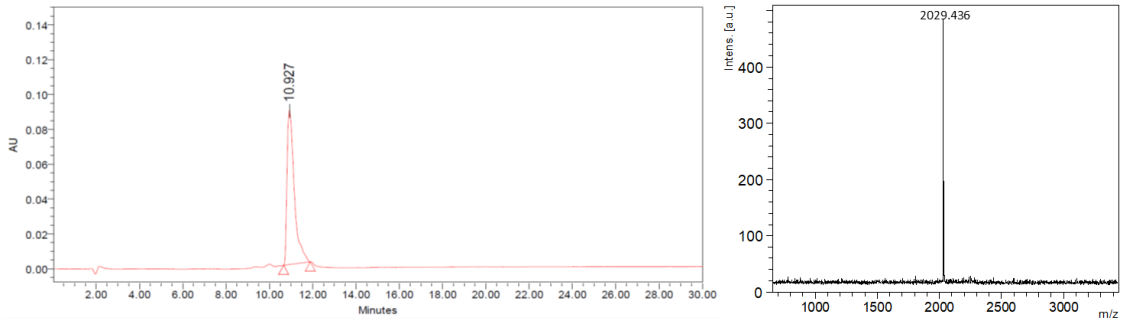

Figure S2.5.1: RP-HPLC profile of H3B10-27 (left) and MALDI-TOF-MS (right).

S2.5.2: Analytical RP-HPLC and MALDI-TOF-MS of purified H3B10-27(13/17F).

RP-HPLC was carried out as described above using the elution gradient: buffer B 30-60% for 30 min, t = 10.712 min.

MALDI-TOF-MS $[M+H]^+$ calculated 2120.422, observed 2121.172.

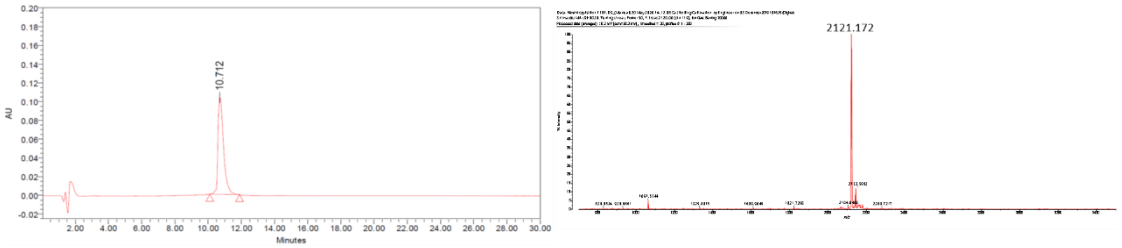

Figure S2.5.2: RP-HPLC profile of H3B10-27(13/17F) (left) and MALDI-TOF-MS (right).

S2.5.3: Analytical RP-HPLC and MALDI-TOF-MS of purified H3B10-27(13/17αF).

RP-HPLC was performed as described above using the elution gradient: buffer B 30-60% for 30 min, t = 13.682 min.

MALDI-TOF-MS $[M+H]^+$ calculated 2148.991, observed 2150.729.

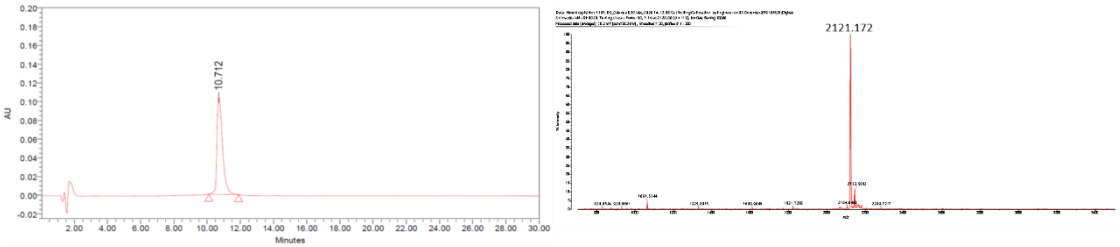

Figure S2.5.3: RP-HPLC profile of H3B10-27(13/17αF) (left) and MALDI-TOF-MS (right).

S2.5: Details of the synthesis and characterization of the target peptide, H3B10-27 (13/17αF)

The target peptide was synthesized using a Biotage (Sweden) Initiator+ Alstra microwave synthesizer. It is difficult to incorporate the sterically demanding α-methylphenylalanine using standard coupling conditions (such as standard 30 min manual coupling at room temperature and HCTU as a coupling reagent). Thus, we used a microwave (25 W), high temperature (75°C), a 4-fold excess of both Fmoc derivative of α-methyl-L-phenylalanine, and HATU as a coupling reagent and a 6-fold excess of base (DIEA) for 10 min (double coupling). We have deprotected the Fmoc group at room temperature (2 x 5 min). It is also important to note that the amino acid next to α-methylphenylalanine is also resistant to standard coupling conditions and therefore the same coupling and deprotection conditions were used for every amino acid after α-methylphenylalanine.

Crude analytical HPLC profile of our target peptide, H3B10-27 (13/17αF):

- Shimadzu Nexera analytical RP-HPLC that incorporates an SPD-M40 UV detector.
- Phenomenex Gemini® C-18 column (250 × 4.6 mm, pore size 110 Å, particle size 5 µm)
- Gradient 20-70% [B] in 15 min

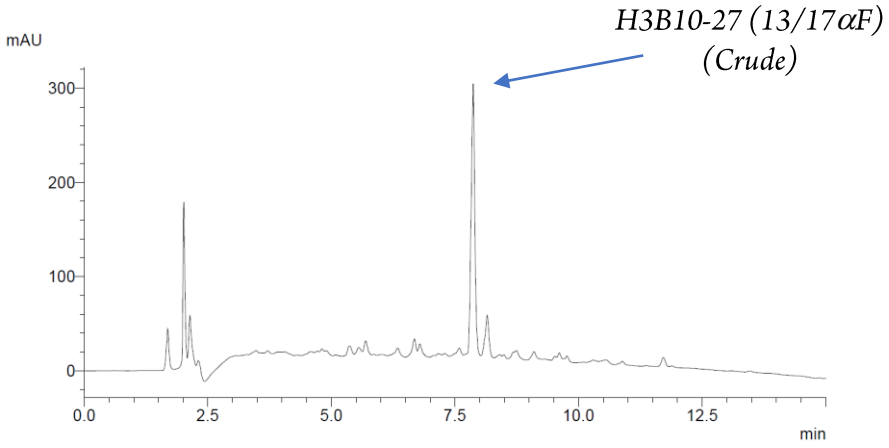

Crude MALDI-TOF MS profile:

Calculated MW: 2148.991

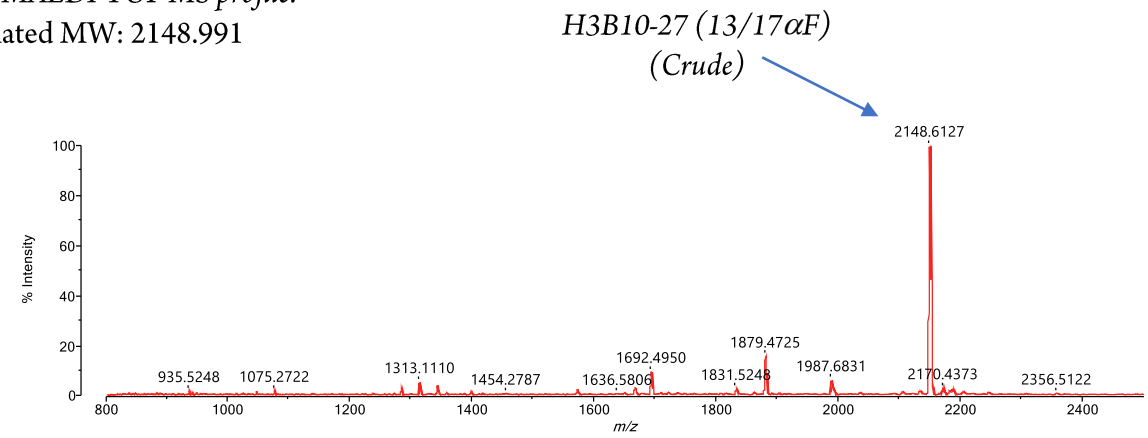

Table S2: MALDI-TOF MS, HPLC purity and yield of peptides

B-Chain Analogue	MALDI TOF MS		HPLC	Purity	Yield
	Observed[1]	Calculated	t_R (min)	(%)	(%)
H3B10-27	2029.436	2026.264	10.927	99	50
H3B10-27(13/17F)	2121.172	2120.422	10.717	>99	67
H3B10-27(13/17αF)	2150.729	2148.991	13.682	>99	60
[1]Observed molecular weights were determined by MALDI-TOF MS of purified peptides					

S2.7: Peptide content determination

Peptide content was determined using Direct Detect® assay-free sample cards and the Direct Detect® spectrometer. All measurements were performed using 2 µL of the sample solution.

S3. CELL-BASED ASSAYS - BINDING AND POTENCY

Since H3 relaxin also binds to and activates the INSL5 receptor, RXFP4, we tested these analogues for RXFP4 binding and activity. An Eu-R3/I5 competition binding assay in CHO-K1-RXFP4 cells revealed that, similar to the HC-stapled Peptide 5, H3B10-27(13/17αF), exhibited strong binding affinity for RXFP4, whereas the control peptides H3B10-27(13/17F) and H3B10-27 had very poor binding affinity (**Figure S3.1 A,C**). Consistent with the binding data, H3B10-27(13/17αF) demonstrated very strong potency at inhibition of cAMP activity at RXFP4, similar to Peptide 5, whereas control peptides exhibited no or poor activity (**Figure S3B,C**). Sections S3.1-S3.2 below describe competition binding and cAMP inhibition methods for both RXFP3 and RXFP4.

(A) Eu-R3/I5 competition binding in RXFP4 cells

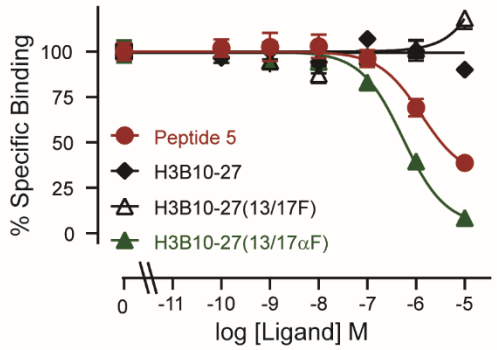

(B) Inhibition of forskolin-induced cAMP activity in RXFP4 cells

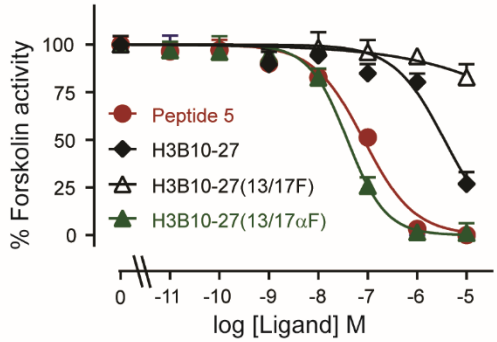

(C) Pooled binding affinity (pKi) and activity (pEC50) on the RXFP4 receptor

	RXFP4	
Ligand	**Eu-R3/I5 pKi**	**cAMP pEC50**
H3 relaxin	8.42 ± 0.19 (4)$^{\#}$	8.94 ± 0.13 (4)$^{\#}$
R3/I5	8.28 ± 0.07 (7)$^{\#}$	8.98 ± 0.09 (8)$^{\#}$
Peptide 5	6.08 ± 0.17 (4)	6.95 ± 0.10 (4)
H3B10-27(13/17αF)	6.81 ± 0.11 (3)$^{\theta}$	7.26 ± 0.12 (3)$^{\theta}$
H3B10-27(13/17F)	No binding (3)	No activity (4)
H3B10-27	<5 (3)	No activity (3)

$^{\#}p<0.001$, $^{\theta}p<0.05$ vs Peptide 5

Figure S3.1. Binding and agonist activity of peptides in CHO-K1-RXFP4 cells. (A) Competition binding curves of increasing concentrations of peptides in competition with 5 nM Eu-R3/I5; (B) Dose-response curves demonstrating inhibition of forskolin induced cAMP activity. Data are the results of 3-4 independent experiments and are expressed as mean ± SEM. (C) Pooled binding affinity (pKi) and cAMP potency (pEC50) data. $^{\#}p<0.001$, $^{\theta}p<0.05$ vs Peptide 5.

S3.1: Details of RXFP3 and RXFP4 binding assays

Chinese hamster ovary CHO-K1 cells stably transfected with RXFP3[4] or RXFP4[5] were plated onto pre-coated, poly-L-lysine 96-well view plates at a density of 50000 cells per well. Medium was aspirated and cells were washed with phosphate-buffered saline (PBS) before competition binding assays were performed with 5 nM Eu-H3B1-22R[6] (RXFP3 ligand) or 5 nM Eu-DTPA-R3/I5[7] (RXFP4 ligand), as described. Competition binding curves for each peptide were performed in triplicate and each experiment was performed independently at least three times. Fluorescent measurements were carried out at excitation of 340 nm and emission of 614 nm on a BMG POLARstar plate reader (BMG Labtech, Melbourne, Australia). Pooled data are presented as mean ± S.E.M. of specific binding and are fitted using a one-site binding curve in GraphPad Prism version 8 (GraphPad Inc., San Diego, USA). Statistical analyses were conducted using one-way analysis of variance with uncorrected Fisher's least significant difference (LSD) post-hoc analysis in GraphPad Prism version 9.

S3.2: RXFP3 and RXFP4 cAMP assays

Peptides were tested for their ability to inhibit forskolin-induced cAMP activity in CHO-K1-RXFP3 or CHO-K1-RXFP4 cells transfected with a pCRE (cAMP Response Element) β-galactosidase reporter plasmid, as described[5,6]. For agonist assays, cells were stimulated with forskolin (5 μM for RXFP3, 1 μM for RXFP4) ± increasing concentrations of each peptide for 6 h. Data were expressed as the % forskolin activity, whereby 100% was defined as forskolin alone and 0% as maximum agonist stimulation (1 μM Analogue 2 for RXFP3 and 1 μM Analogue 13 for RXFP4). Data were analysed and plotted using GraphPad Prism 9 and are expressed as the mean ± SEM of the pooled data. Statistical analysis was conducted using one-way ANOVA with Uncorrected Fisher's LSD post-hoc analysis using GraphPad Prism 9.

S3.3: NanoBRET β-arrestin recruitment assays

It has been demonstrated that agonist activation of RXFP3[8] and RXFP4[9] results in the recruitment of both β-arrestin1 and β-arrestin2, leading to receptor internalization. We assessed if H3B10-27(13/17αF) retained the ability to recruit β-arrestin2 and therefore display full agonist activity at RXFP3 and RXFP4, in comparison to Peptide 5. In this study, we developed a more sensitive β-arrestin2 recruitment assay using Nanoluciferase (NLuc)-tagged RXFP3 (RXFP3-NLuc) and Venus-tagged-β-arrestin2 (Venus-β-Arr2) in a similar manner to that used for RXFP4[10].

We first demonstrated that the RXFP3-NLuc construct signalled in response to an RXFP3 agonist, R3/I5, with identical potency and efficacy to responses on untagged RXFP3 (Figure S3.3.1). We then tested if R3/I5 was able to stimulate a dose-dependent increase in NanoBRET signal in cells co-transfected with Venus-β-Arr2 (Figure S3.3.2 (A)) As anticipated, the BRET signals obtained were more robust than those with rLuc8 and demonstrated a clear ligand-mediated concentration dependence. The responses to Peptide 5 and H3B10-27(13/17αF) were tested in parallel with both peptides displaying dose-dependent recruitment of Venus-β-Arr2 with similar efficacy to R3/I5 (Figure S3.3.2 B,C).

Notably, when Peptide 5 and H3B10-27(13/17αF) were tested in parallel with R3/I5 in RXFP4-NLuc/Venus-β-Arr2 recruitment assays, there were marked differences in peptide activity compared to R3/I5 (Figure S3.3.3)[9].

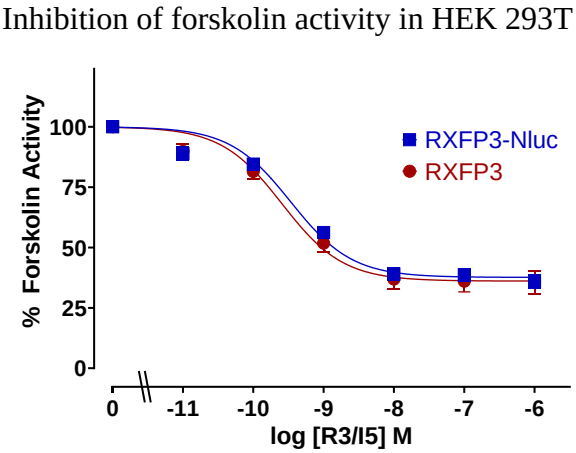

Figure S3.3.1: RXFP3-NLuc construct signalled in response to an RXFP3 agonist, R3/I5, with identical potency and efficacy compared to untagged RXFP3.

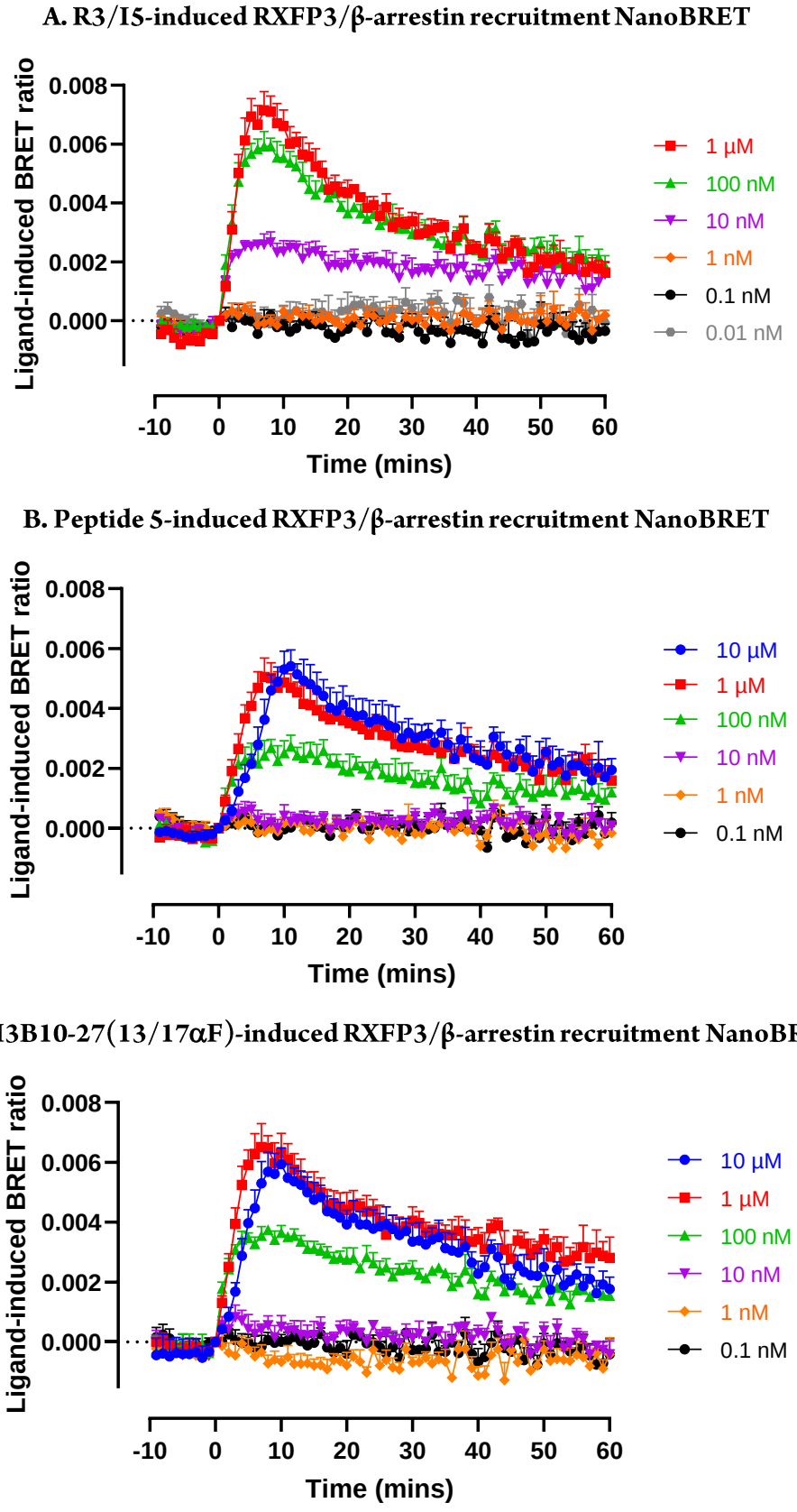

Figure S3.3.2. Ligand-induced β-arrestin recruitment measured by NanoBRET between nanoluciferase-tagged RXFP3 (RXFP3-NL) and Venus-tagged-β-arrestin2 (β-Arr2-Venus). Real-time NanoBRET measurement of the dose-dependent (A) R3/I5 (B) Peptide 5 and (C) H3B10-27(13/17αF) induced interaction of RXFP3-NL and β-Arr2-Venus.

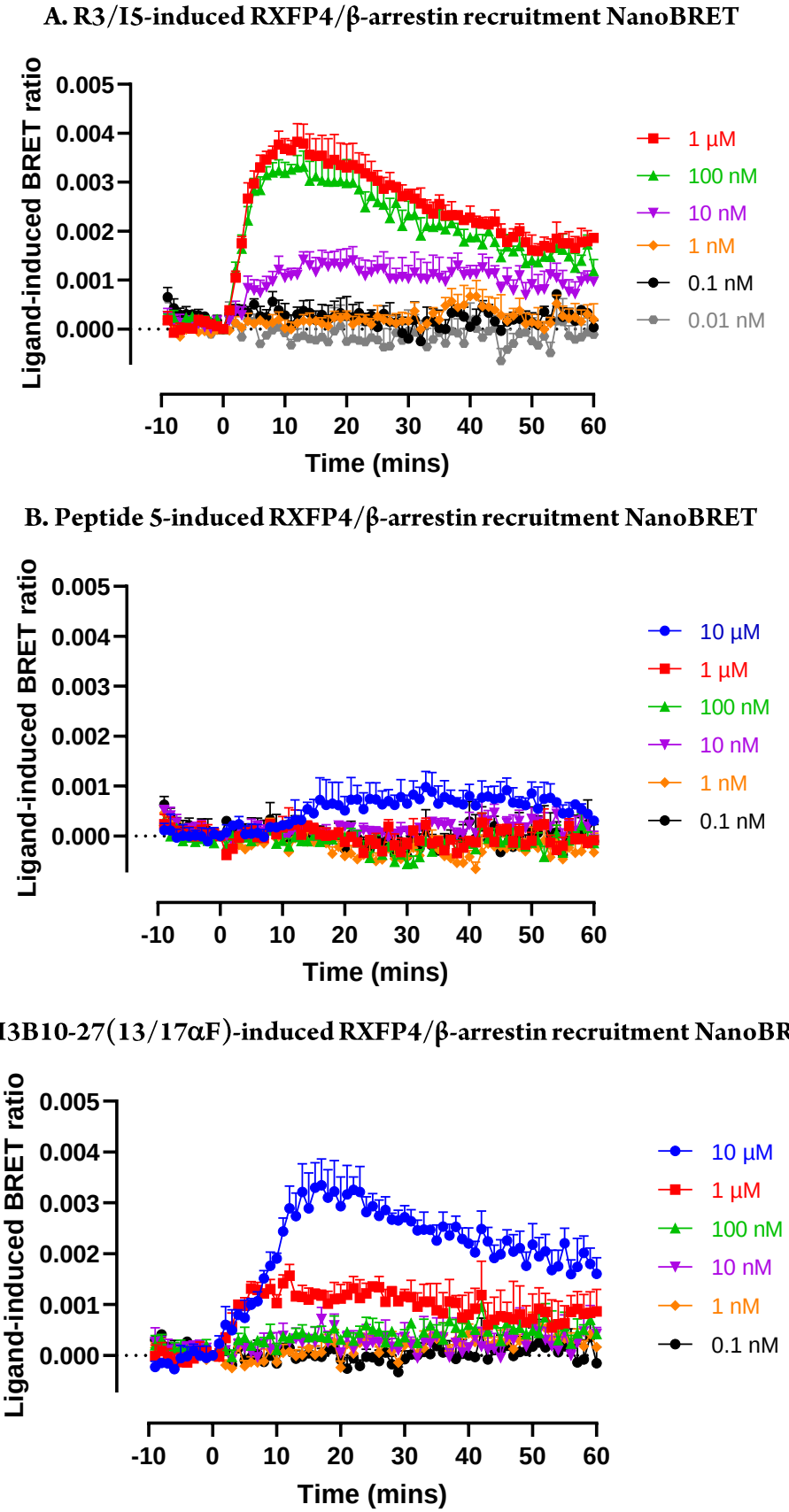

Figure S3.3.3. Ligand-induced β-arrestin recruitment measured by NanoBRET between nanoluciferase-tagged RXFP4 (RXFP4-NL) and Venus-tagged-β-arrestin2 (β-Arr2-Venus). Real-time NanoBRET measurement of the dose-dependent (A) R3/I5 (B) Peptide 5 and (C) H3B10-27(13/17αF) induced interaction of RXFP4-NL and β-Arr2-Venus.

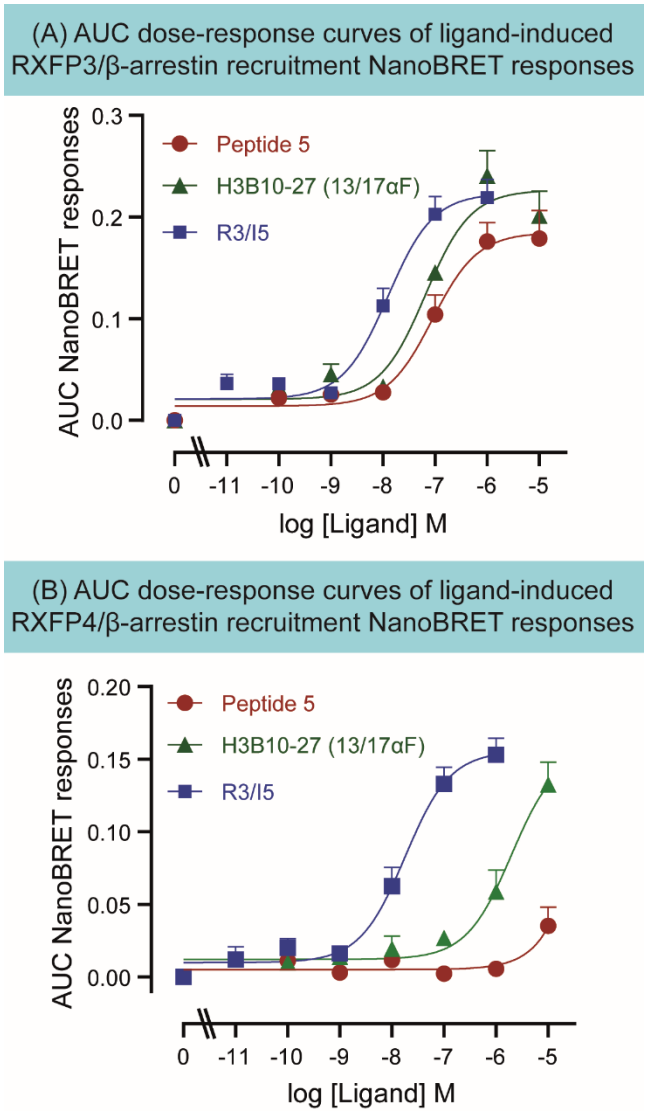

Figure S3.3.4. Ligand induced β-arrestin2 recruitment. Area under the curve (AUC) dose-response curves of ligand-induced (A) RXFP3/β-arrestin recruitment NanoBRET responses, (B) RXFP4/β-arrestin recruitment NanoBRET responses.

Dose-response curves were plotted based on the area under the curve (AUC) of the entire time course (from Figure 3.3.2) and demonstrated that both Peptide 5 (pEC50 = 7.19 ± 0.16, $p<0.05$) and H3B10-27(13/17 α F) (pEC50 = 7.05 ± 0.17, $p<0.01$) displayed similar, slightly lower potency compared to R3/I5 (pEC50 = 7.91 ± 0.13) (Figure 3.3.4A and Table S2) consistent with their slightly lower affinity and potency in cAMP activity assays.

Dose-response curves were plotted based on the AUC of the entire time course (from Figure 3.3.3) and demonstrated that Peptide 5 produced only a minimal response at the maximum 10 μM concentration, whereas H3B10-27(13/17 α F) was 100-fold less potent than R3/I5 (pEC50 = 5.57 ± 0.26, compared to pEC50 = 7.56 ± 0.16, $p<0.001$) (Figure 3.3.4B and Table S2). Together, these binding and activity data suggest our novel analogue H3B10-27(13/17αF) can mimic the biological actions of HC-stapled Peptide 5 in both RXFP3- and RXFP4-expressing cells. However, the lower affinity and potency of both peptides on RXFP4 correlates with a lower potency in β-arrestin2 recruitment. Detailed methods and data for NanoBRET β-arrestin recruitment assays are included in section S3.4 below.

S3.4: NanoBRET β-arrestin recruitment assays

Previous studies utilizing RXFP3 or RXFP4 C-terminally tagged with Renilla Luciferase 8 and Venus-tagged-β-arrestin1/2 have demonstrated that activation of RXFP3[8] and RXFP4[9] leads to the recruitment of both β-arrestin1 and β-arrestin2, leading to receptor internalization[8]. We previously developed a more sensitive NanoBRET β-arrestin2 recruitment assay by fusing Nanoluciferase at the C-terminus of RXFP4 (RXFP4-NLuc) and co-transfecting with Venus-tagged-β-arrestin2 (β-Arr2-Venus)[10]. In this study we developed an RXFP3 β-arrestin2 recruitment assay by PCR cloning NLuc onto the C-terminus of human RXFP3 in an identical manner to the RXFP3-rLuc8 construct to create pcDNA3.1-RXFP3-NLuc[8]. The construct was sequenced on both strands to confirm that the NLuc was in frame with RXFP3 and there were no additional PCR mutations. pcDNA3.1-RXFP3-NL was tested in parallel with pcDNA3.1-RXFP3 in cAMP activity assays to determine if the C-terminal nanoluciferase fusion affected agonist activity. Hence constructs were co-transfected in HEK 293T cells with the pCRE-β-galactosidase reporter, as described above, and stimulated with the RXFP3 agonist, R3/I5.

For NanoBRET β-arrestin2 recruitment assays, HEK293T cells were plated onto a six-well plate, and were transfected the following day with β-arrestin2-Venus and either RXFP3-Nluc or RXFP4-Nluc, in the pcDNA3.1/Zeo(+) vector, using Lipofectamine 2000. The next day, cells were washed with PBS and resuspended in complete media containing 25 mM HEPES but no phenol red and were seeded into a 96-well CulturPlate (PerkinElmer). The next day, prior to the assay, cells were pre-incubated in phenol red free media with NLuc substrate, 5 μM coelenterazine 400a for RXFP3-nLuc and 5 μM coelenterazine h for RXFP4-NLuc (both from Nanolight, Pinetop, AZ, USA) to establish a baseline, before addition of ligand or vehicle. Emissions were detected simultaneously using a PHERAstar FSX plate reader (BMG Labtech) with 450/80 nm and 535/30 nm filters.

Ligand-induced BRET ratio was calculated by subtracting the ratio of 535/30 nm emissions to 450/80 nm emissions for vehicle from the same ratio for ligand-treated wells. For time-courses, ligand-induced BRET ratio was plotted against time, with the last pre-reading before ligand addition displayed as the zero-time point (time of vehicle/ligand addition). Data are representative of 3-5 experiments performed in duplicate and concentration-response curves were fit to data by applying non-linear regression to area under the curve of time-course data, using GraphPad Prism 9.

Table S3: Pooled ligand-induced β-arrestin2 recruitment potency (pEC50).

Ligand	RXFP3 pEC50	RXFP4 pEC50
R3/I5	7.91 ± 0.13 (n = 4)	7.56 ± 0.16 (n = 4)
B10-27(13/17αF)	7.19 ± 0.16$^{\#}$ (n = 4)	5.57 ± 0.26$^{\#\#\#}$ (n = 3)
Peptide 5 (B10-27(13/17HC))	7.05 ± 0.17$^{\#\#}$ (n = 4)	<5 (n = 3)

$^{\#}p<0.05$, $^{\#\#}p<0.01$, $^{\#\#\#}p<0.001$ vs R3/I5; Unpaired t-tests.

S4. SOLUTION NMR SPECTROSCOPY

All NMR experiments were routinely collected at 15°C on a 700 MHz Bruker Advance HDIII spectrometer equipped with triple resonance cryoprobe. Peptide (2 mg) was dissolved in 0.5 mL of 90% H_2O–10% D_2O imidazole-d_4 buffer at ~pH 6.8. Two-dimensional data sets including a homonuclear proton TOCSY (1024 × 256 complex points) with a mixing time of 80 ms, ^{1}H-^{1}H NOESY (1024 × 256 complex points) with a mixing time of 200 ms and a ^{1}H–^{15}N HSQC (1024 × 256 complex points) at natural abundance were recorded. Spectra were processed using NMRPipe and typically Fourier-transformed after applying Lorentz-to-Gauss window functions in the direct dimension and cosine bells in the indirect dimensions. NMR data were analysed using SPARKY[11-15].

For H3 B10-27αF peptide structure determination, ~60 sequential (i, i+1 and 1-i+2 or greater, Table S4.1) cross peaks in the ^{1}H-^{1}H NOESY spectrum were picked, assigned and integrated using Sparky and translated into interproton distances using CYANA. A pool of 100 three-dimensional structures were generated using torsion angle dynamics protocol (~18 torsion angles, Table S4.2) and only 20 structures with the lowest CYANA target function (0.08 ± 0.01 Å^2, Table S4.2) were selected to best represent the structure of our target peptide.

Table S4.1 1H assignments of the H3 B10-27αF peptide at 15°C and pH 6.8

	NH	Hα	Hβ	Hγ	Hδ	Hε	other
S10	-	4.14	3.95				
G11	8.79	4.08,4.02					
R12	8.46		4.17	1.66	1.53		3.14
X13	8.18	-	3.10, 2.96		6.85	7.26	1.36 ($H_3\beta$)
F14	7.58	4.40	3.03		7.17		
I15	7.80	3.97	1.84	1.48,1.15		0.840 ($H_3\gamma$)	
R16	7.97	4.10	1.63,1.58		1.45		3.08
X17	7.84	-	3.13		7.08	7.32	1.36 ($H_3\beta$)
V18	7.63	3.88	1.95				0.78, 0.87 ($H_3\gamma$)
I19	8.02	3.98	1.79	1.43,1.12		0.75 ($H_3\gamma$)	
F20	8.20		4.61	3.08, 2.90			7.16
T21	8.04	4.27	4.13				1.07 ($H_3\gamma$)
S22	8.23	4.40	3.92,3.87				
G23	8.38	3.96					
S25	8.19	4.33	3.72				
R26	8.19	4.22	1.62,1.49	1.36		3.00	
W27	7.83	4.58	3.32,3.13	7.17 (Hδ1)	10.04 (Hε1)	7.60 (Hη2)	7.43 (Hζ2) 7.139 (Hζ)

Table S4.2. Structural statistics for the best 20 structures of H3 B10-27αF peptide from a trial calculation of 100 structures.

No. distance constraints	
Intraresidue	37
sequential (i, i+1)	52
shortrange (i, >i+2)	8
No. torsion angle constraints (ϕ, φ)	18
Cyana target function (Å^2)*	0.08 ± 0.01
Maximum distance violation (Å)	0.16
Maximum angle violation (°)	0
Backbone atom rmsd (Å)	
Residues 12-23	0.77 ± 0.24
Ramachandran plot regions (%) (non-glycine)	
Most favored	92.3
Allowed region	7.7

* 13 VdW violations due to the unnatural CH_3 substituent on the Cα of residues 13 and 17 and their neighbouring residues.

S5. *IN VITRO* SERUM STABILITY ASSAY

Human serum (400 µL) was mixed with 200 µg peptide dissolved in 100 µL of water at 37°C. Eighty (80) µl of sample was removed at various time points (0 min, 30 min, 60 min, 120 min, 240 min, and 480 min), and 160 µL of acetonitrile added to precipitate plasma proteins. The solution was then centrifuged at 12000 rpm for 15 min at 4°C. 200 µL of supernatant was taken and mixed with 240 µL of milli-Q water and each sample analysed by RP-HPLC (2 × 80 µL injection) by measuring the area under the peak at appropriate retention times compared to the peak area of the peptide at time zero (100%). Data analysis (n = 3, duplicate) was performed using a non-linear fit one-phase decay model in GraphPad Prism 9.

S6. STUDIES OF *EX VIVO* PERFUSED RAT BRAINSTEM

Juvenile Sprague-Dawley rats (postnatal day 18–23, weighing 40–60 g) were used. Rats were maintained on a 12 h light/dark cycle with food and water available *ad libitum*. All experiments followed protocols approved by The Florey Institute of Neuroscience and Mental Health Animal Ethics Committee and performed in accordance with the NHMRC Code of Practice for the Use of Animals for Scientific Purposes. We followed recently published methods[16].

Briefly, rats were deeply anaesthetized via inhalation of isoflurane (Zoetis, Sydney, Australia) until complete loss of the hindpaw withdrawal reflex in response to noxious pinch. They were bisected below the diaphragm, and immediately immersed in ice-cold Ringer's solution, skinned, eviscerated and decerebrated at the pre-collicular level. The right thoracic phrenic nerve was isolated and cut distally at the level of its insertion into the diaphragm muscle to record the efferent activity. The heart and lungs were removed and the preparation was transferred to a recording chamber. A double-lumen catheter was inserted into the descending aorta for retrograde perfusion of carbogenated Ringer's solution, heated to 31°C using a peristaltic pump (Watson & Marlow 505 S, Falmouth, UK). The second lumen of the catheter was used to monitor aortic perfusion pressure, which was maintained in the range 40–70 mm Hg by adjusting the flow 18–22 mL/min. The perfusate was an isosmotic Ringer's solution containing, in mM: NaCl, 125.00; $NaHCO_3$, 24.00; KCl, 3.00; $CaCl_2$, 2.50; $MgSO_4$, 1.25; KH_2PO_4, 1.25; and glucose, 10.00)

containing an oncotic agent (0.45% sucrose), bubbled with carbogen (95% O_2 and 5% CO_2), pH 7.4 after carbogenation, and filtered using a nylon screen (pore size 100 μm; Millipore, Tullagreen, Ireland). After respiratory-related movements commenced, a neuromuscular blocker (vecuronium bromide, 300 μg/200 mL perfusate, Mylan, Brisbane, Australia) was added to the perfusate to mechanically stabilize the preparation. The eupneic respiratory pattern was obtained by stimulating the peripheral chemoreflex with a bolus injection of NaCN (100 μL, 0.1% w/v).

The phrenic nerve activity (PNA) was recorded from the cut proximal nerve end using a suction electrode. The signal was amplified (differential amplifier DP-311, Warner instruments, Hamden, USA), band-pass filtered from 100 Hz to 10 kHz, digitized (PowerLab/16SP ADInstruments, Sydney Australia) and then viewed and recorded using LabChart (version 7.0, ADInstruments).

After the preparation stabilized, a minimum of 10 min baseline activity was recorded. Then, the peripheral chemoreflex was evoked at least 2 times by a bolus injection of NaCN (100 μL, 0.1% w/v) under control conditions. At 5 min after the last control chemoreflex stimulus, H3B10-27(13/17αF) was added to the perfusate (2 μM final concentration). Following an 8-10 min interval, the chemoreflex stimuli were repeated, as described.

Analyses of the PNA were performed using Spike2 software version 7.12 (Cambridge Electronic Design, Cambridge, UK). The phrenic nerve burst frequency was analysed over a 1 min period during the baseline recording and after the systemic application of H3B10-27(13/17αF), immediately before the second chemoreflex stimulus. The respiratory response to the chemoreflex was analysed by counting the number of phrenic nerve bursts during the tachypneic response. Results are expressed as the mean ± SEM and analysed by paired t-test, using SigmaPlot statistics software 11.0. The level of significance used was $p \leq 0.05$.

S7. *IN VIVO* FEEDING STUDIES IN RATS

Male, adult Sprague-Dawley rats (n = 29, weighting 250–300 g; Janvier Labs, Le Genest-Saint-Isle, France) were used. Rats were housed under ambient conditions (21°C) and maintained on a 12 h light/dark cycle (lights on 08:00–20:00), with access to food (laboratory chow) and water *ad libitum*. Rats were acclimatized to the animal facility for at least 1 week before further treatment. Experiments were conducted with the approval of the Committee of Ethics in Animal Welfare of the Universitat Jaume I and registered in the Conselleria de Agricultura of the Generalitat Valenciana (Spain). All efforts were made to minimize the number of animals used and special attention was taken to minimize any suffering or discomfort.

Rats were anesthetized with isoflurane (Isoflutek®, Laboratorios Karizoo, Barcelona, Spain) for the implantation of cannula into the lateral ventricle. An initial anesthesia was induced with 4% isoflurane in oxygen, 2 L/min, and under deep anesthesia, rats were placed in a stereotaxic frame (David Kopf Instruments, Tujunga, CA, USA) and maintained with 2–3% isoflurane in oxygen, 200 mL/min. The skull was positioned, and a stainless-steel guide cannula (22 gauge) was implanted with the cannula tip aimed at the lateral ventricle (coordinates: anteroposterior, 0.2 mm; mediolateral, −1.5 mm; dorsolateral, −3.7 mm). Th e cannula was attached to the skull using surgical screws and dental cement. When recovered, rats were placed individually in clean cages. Meloxicam (Metacam® Boehringer Ingelheim Vetmedica GmbH, Rhein, Germany) was subcutaneously injected at a dosage of 0.5 mg in 0.1 mL (for 2 days), to provide acute and ongoing post-operative analgesia. Rats were single-housed and allowed to recover for 7 days, during which they were handled and weighed daily to habituate them to the experimenter. A dummy stylet of stainless steel wire (30 gauge) was inserted into each cannula to maintain patency.

Lateral cerebral ventricle infusions were made using a 30-gauge stainless steel hypodermic tubing injector (Plastics One, East Virginia, USA) connected to a 10-μL Hamilton microsyringe (Hamilton Instruments, Reno, NV, USA) by polyethylene tubing (0.80 mm outer and 0.40 mm internal diameter; Plastics One). On post-surgery day 3, correct positioning of the cannula was verified in each rat by injecting 5 μL of a 2 ng/μL solution of angiotensin II (Hello Bio HB3488, Dunshlaughlin, Ireland) in artificial cerebrospinal fluid [aCSF; made from stock of 10× aCSF (1470 mM NaCl, 40 mM KCl, 8.5 mM $MgCl_2$, and 23 mM $CaCl_2$)], and observing if this produced a dipsogenic response, defined as repeated drinking episodes of ≥5 s that commenced within 1 min of angiotensin II administration.

Each rat received 3 icv infusions on days 7, 12 and 15 post-surgery. Rats were handled 3 days before the infusions started and left in the infusion room on the previous day. Infusions were performed 2 h after lights on. The injection volume was 5 μL in all cases and contained either aCSF (n = 8), 0.1 nmol H3B10-27(13/17αF) (n = 10), 0.5 nmol H3B10-27(13/17αF) (n = 10), 1 nmol B10-27(13/17αF) (n = 14), 4 nmol H3B10-27(13/17αF) (n = 12) or 1 nmol A2 (n = 15) in 6 groups of injections in total. A pre-weighed water bottle was also placed in its usual compartment. Food and water were weighed at intervals of 15, 30, 60 and 120 min after the infusion. Thereafter, the cages were returned to the home room.

At the end of the experiment, rats were anesthetized with an overdose of 125 mg/kg sodium pentobarbital (Dolethal, Vetaquinol, Madrid, Spain) to check cannula placement. Rats were transcardially-perfused with saline, followed by 4% paraformaldehyde in 0.1 M phosphate buffer. Brains were removed from the skull and kept in the same fixative overnight at 4°C, then transferred to 30% sucrose in 0.01M phosphate buffer saline for cryoprotection. Brains were coronally sectioned with a sliding microtome and examined.

Food and water intake data were analyzed using GraphPad Prism 5. Results are expressed as mean ± SEM. A D'Agostino and Pearson normality test was applied. Under normality conditions an unpaired t test was applied to compare groups. When normality was not achieved, a non-parametric Mann-Whitney U test was applied to compare between medians. The level of significance used was $\alpha = 0.05$.

Figure S7. Exemplary illustration of cannula placement targeting the lateral ventricle in a frozen section (asterisks). Calibration bar 1 mm.

S8. CHEMICAL SYNTHESIS: H3 RELAXIN vs H3B10-27(13/17αF)

Chemical synthesis of H3 relaxin and HC-stapled Peptide 5 is tedious and laborious compared with H3B10-27(13/17αF) (Figure S8). Our B-chain-only analogue, H3B10-27(13/17αF) (18 residues) was very high yielding (~60%) compared with both H3 relaxin (51 residues, yield less than 2% starting from the A-chain, 5.7% starting from the B-chain[17]) and HC-stapled Peptide 5 (18 residues, yield, ~10%). While the HC-stapled Peptide 5 has an unknown (*E/Z*) conformation and is insoluble in water, our novel RXFP3 agonist, H3B10-27(13/17αF), is a single species and water soluble (Figure S8).

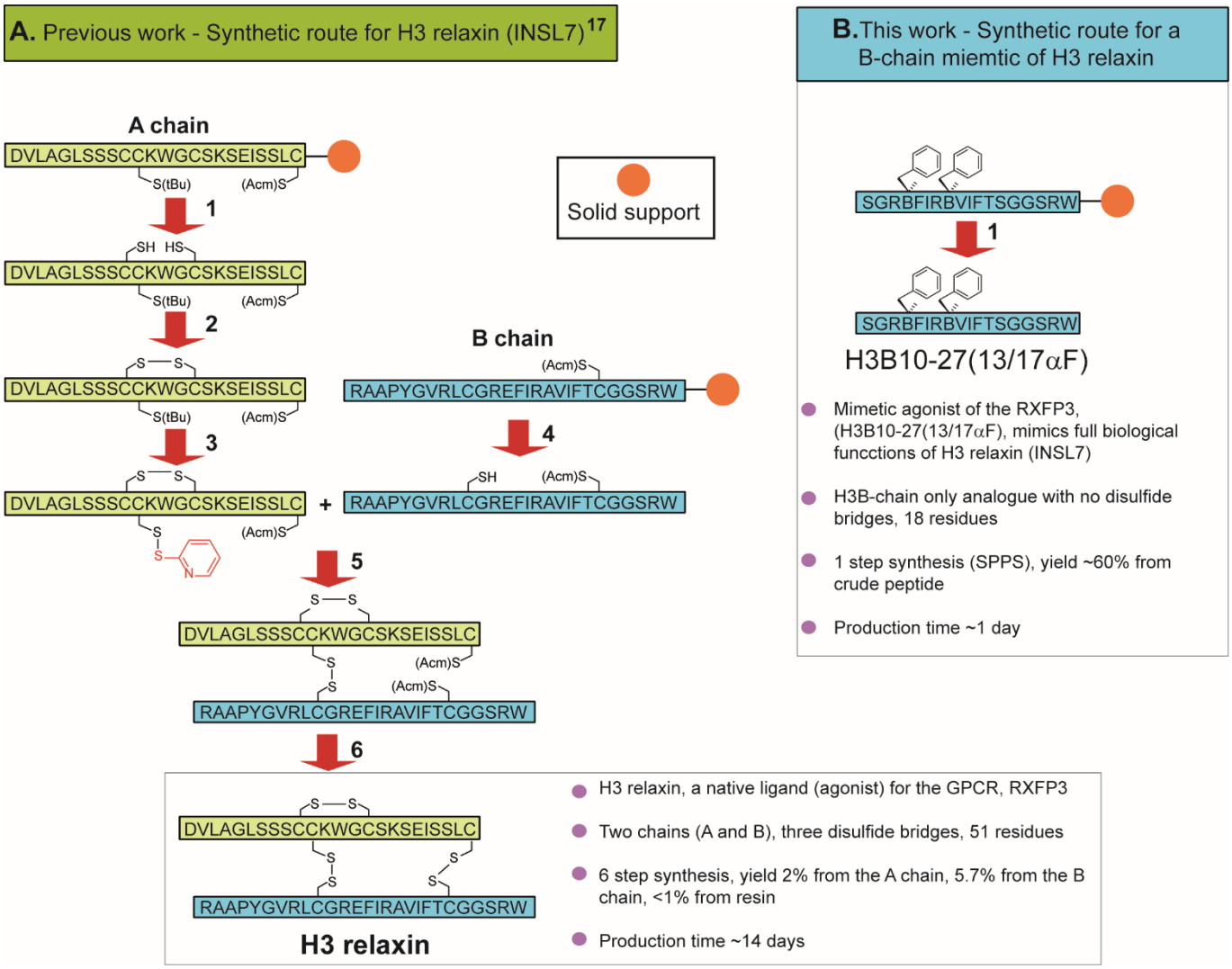

Figure S8. Comparison of chemical synthetic routes. (A) The synthesis of the two chain H3 relaxin requires assembly of two separate chains (A and B chains), four separate reactions for the regioselective formation of its disulfide bonds, and six purification steps, resulting in low overall yields[33]. (B) In contrast H3B10-27(13/17αF) is directly assembled in its final form on resin, requiring a single purification step after cleavage.

REFERENCES

1. Haugaard-Jonsson, L. M.; Hossain, M. A.; Daly, N. L.; Bathgate, R. A.; Wade, J. D.; Craik, D. J.; Rosengren, K. J., Structure of the R3/I5 chimeric relaxin peptide, a selective GPCR135 and GPCR142 agonist. *J Biol Chem* **2008,** *283*, 23811-8.
2. Shabanpoor, F.; Akhter Hossain, M.; Ryan, P. J.; Belgi, A.; Layfield, S.; Kocan, M.; Zhang, S.; Samuel, C. S.; Gundlach, A. L.; Bathgate, R. A.; Separovic, F.; Wade, J. D., Minimization of human relaxin-3 leading to high-affinity analogues with increased selectivity for relaxin-family peptide 3 receptor (RXFP3) over RXFP1. *J Med Chem* **2012,** *55*, 1671-81.
3. Hojo, K.; Hossain, M. A.; Tailhades, J.; Shabanpoor, F.; Wong, L. L.; Ong-Palsson, E. E.; Kastman, H. E.; Ma, S.; Gundlach, A. L.; Rosengren, K. J.; Wade, J. D.; Bathgate, R. A., Development of a single-chain peptide agonist of the relaxin-3 receptor using hydrocarbon stapling. *J Med Chem* **2016,** *59*, 7445-56.
4. Van der Westhuizen, E. T.; Sexton, P. M.; Bathgate, R. A.; Summers, R. J., Responses of GPCR135 to human gene 3 (H3) relaxin in CHO-K1 cells determined by microphysiometry. *Ann N Y Acad Sci* **2005,** *1041*, 332-7.
5. Belgi, A.; Hossain, M. A.; Shabanpoor, F.; Chan, L.; Zhang, S.; Bathgate, R. A.; Tregear, G. W.; Wade, J. D., Structure and function relationship of murine insulin-like peptide 5 (INSL5): free C-terminus is essential for RXFP4 receptor binding and activation. *Biochemistry* **2011,** *50*, 8352-61.
6. Haugaard-Kedstrom, L. M.; Wong, L. L.; Bathgate, R. A.; Rosengren, K. J., Synthesis and pharmacological characterization of a europium-labelled single-chain antagonist for binding studies of the relaxin-3 receptor RXFP3. *Amino Acids* **2015,** *47*, 1267-71.
7. Zhang, X.; Bathgate, R. A. D.; Hossain, M. A., Human Insulin-like peptide 5 (INSL5). Identification of a simplified version of two-chain analog A13. *ACS Med Chem Lett* **2020,** *11*, 2455-60.
8. Kocan, M.; Sarwar, M.; Hossain, M. A.; Wade, J. D.; Summers, R. J., Signalling profiles of H3 relaxin, H2 relaxin and R3(BΔ23-27)R/I5 acting at the relaxin family peptide receptor 3 (RXFP3). *Br J Pharmacol* **2014,** *171*, 2827-41.
9. Ang, S. Y.; Hutchinson, D. S.; Patil, N.; Evans, B. A.; Bathgate, R. A. D.; Halls, M. L.; Hossain, M. A.; Summers, R. J.; Kocan, M., Signal transduction pathways activated by insulin-like peptide 5 at the relaxin family peptide RXFP4 receptor. *Br J Pharmacol* **2017,** *174*, 1077-89.
10. Pustovit, R. V.; Zhang, X.; Liew, J. J.; Praveen, P.; Liu, M.; Koo, A.; Oparija-Rogenmozere, L.; Ou, Q.; Kocan, M.; Nie, S.; Bathgate, R. A.; Furness, J. B.; Hossain, M. A., A novel antagonist peptide reveals a physiological role of insulin-like peptide 5 in control of colorectal function. *ACS Pharmacol Transl Sci* **2021,** *4*, 1665-74.
11. Mayzel, M.; Rosenlow, J.; Isaksson, L.; Orekhov, V. Y., Time-resolved multidimensional NMR with non-uniform sampling. *J Biomol NMR* **2014,** *58*, 129-39.
12. Kazimierczuk, K.; Orekhov, V. Y., Accelerated NMR spectroscopy by using compressed sensing. *Angew Chem Int Ed Engl* **2011,** *50*, 5556-9.
13. Delaglio, F.; Grzesiek, S.; Vuister, G. W.; Zhu, G.; Pfeifer, J.; Bax, A., NMRPipe: a multidimensional spectral processing system based on UNIX pipes. *J Biomol NMR* **1995,** *6*, 277-93.
14. Lee, W.; Tonelli, M.; Markley, J. L., NMRFAM-SPARKY: enhanced software for biomolecular NMR spectroscopy. *Bioinformatics* **2015,** *31*, 1325-7.
15. Guntert, P., Automated NMR structure calculation with CYANA. *Methods Mol Biol* **2004,** *278*, 353-78.

16. Furuya, W. I.; Dhingra, R. R.; Gundlach, A. L.; Hossain, M. A.; Dutschmann, M., Relaxin-3 receptor (RXFP3) activation in the nucleus of the solitary tract modulates respiratory rate and the arterial chemoreceptor reflex in rat. *Respir Physiol Neurobiol* **2020**, *271*, 103310.
17. Bathgate, R. A.; Lin, F.; Hanson, N. F.; Otvos, L., Jr.; Guidolin, A.; Giannakis, C.; Bastiras, S.; Layfield, S. L.; Ferraro, T.; Ma, S.; Zhao, C.; Gundlach, A. L.; Samuel, C. S.; Tregear, G. W.; Wade, J. D., Relaxin-3: improved synthesis strategy and demonstration of its high-affinity interaction with the relaxin receptor LGR7 both in vitro and in vivo. *Biochemistry* **2006,** *45*, 1043-53.